Received 29 June 2021
Revised 26 October 2021
Accepted 30 November 2021

Simulation of iron losses in induction machines using an iron loss model for rotating magnetization loci in no electrical steel

Martin Marco Nell, Benedikt Schauerte, Tim Brimmers and Kay Hameyer
Institute of Electrical Machines (IEM), RWTH Aachen University, Aachen, Germany

Abstract

Purpose – Various iron loss models can be used for the simulation of electrical machines. In particular, the effect of rotating magnetic flux density at certain geometric locations in a machine is often neglected by conventional iron loss models. The purpose of this paper is to compare the adapted IEM loss model for rotational magnetization that is developed within the context of this work with other existing models in the framework of a finite element simulation of an exemplary induction machine.

Design/methodology/approach – In this paper, an adapted IEM loss model for rotational magnetization, developed within the context of the paper, is implemented in a finite element method simulation and used to calculate the iron losses of an exemplary induction machine. The resulting iron losses are compared with the iron losses simulated using three other already existing iron loss models that do not consider the effects of rotational flux densities. The used iron loss models are the modified Bertotti model, the IEM-5 parameter model and a dynamic core loss model. For the analysis, different operating points and different locations within the machine are examined, leading to the analysis of different shapes and amplitudes of the flux density curves.

Findings – The modified Bertotti model, the IEM-5 parameter model and the dynamic core loss model underestimate the hysteresis and excess losses in locations of rotational magnetizations and low-flux densities, while they overestimate the losses for rotational magnetization and high-flux densities. The error is reduced by the adapted IEM loss model for rotational magnetization. Furthermore, it is shown that the dynamic core loss model results in significant higher hysteresis losses for magnetizations with a high amount of harmonics.

Originality/value – The simulation results show that the adapted IEM loss model for rotational magnetization provides very similar results to existing iron loss models in the case of unidirectional magnetization. Furthermore, it is able to reproduce the effects of rotational flux densities on iron losses within a machine simulation.

Keywords Electrical machines, Iron loss modeling, Induction machine, Finite element analysis, Rotational magnetization, Iron losses

Paper type Research paper

COMPEL - The international journal for computation and mathematics in electrical and electronic engineering
Vol. 41 No. 2, 2022
pp. 600-614

0332-1649
DOI 10.1108/COMPEL-06-2021-0220

1. Introduction

Quantifying the efficiency of electrical machines by simulation requires accurate loss models already at the development stage. In particular, the iron losses gain importance for magnetically highly stressed machines and high-speed applications. Iron losses are strongly

dependent on the operating point of the machine, as the various loss components depend on the magnetic flux density and frequency. In addition to the dependence on the operating point, the iron loss density also varies within the machine itself. The flux density locations vary from place to place within the machine (Nell *et al.*, 2021), resulting in different forms of local magnetizations such as alternating, elliptical, or rotating. In studies by Ragusa *et al.* (2007) and Appino *et al.* (2009), it is shown that these different forms of flux density also have a great influence on the iron losses inside the steel sheets.

Different modeling approaches are commonly used to model the iron losses in the stator and rotor laminations of an electrical machine. In a study by Krings and Soulard (2010), an overview of existing iron loss models is given. In addition, these models are compared with respect to their accuracy, applicability for different excitation modes and parameterization efforts. The methods for calculating iron losses can be divided into frequency-domain and time-domain methods. In a study by Kowal *et al.* (2015), two frequency-domain and one time-domain methods are used to calculate iron losses under alternating sinusoidal and nonsinusoidal magnetization, and their results are analyzed and compared. Also, in a study by Zhu *et al.* (2019), several time- and frequency-based models are analyzed under the assumption of sinusoidal and nonsinusoidal magnetization. The majority of the models listed there are subject to the assumption of unidirectional magnetization or flux densities.

The iron losses of an electrical steel sheet differ for alternating, elliptical and rotating magnetization, as shown in Ragusa *et al.* (2007) and Appino *et al.*(2009). The differences are dependent on the frequency, the magnetic flux density and the axis ratio of the flux density loci. To consider such rotational magnetizations, Zhu *et al.* (2019) and Abdi *et al.*(2021) suggested to divide the field trajectories for the calculation of the losses into two components, the rolling and transverse direction. As shown by Ragusa *et al.* (2007) and Appino *et al.* (2009), the hysteresis losses and excess losses for low values of flux densities ($B < 1.5\,\mathrm{T}$) increase by increasing axis ratio between the maximum flux density in the rolling and transverse direction. This effect results in higher hysteresis and excess losses for rotating magnetizations compared to alternating ones. For flux density above a certain high value ($B > 1.5\,\mathrm{T}$), the hysteresis and excess losses for rotating magnetizations begin to decrease, whereas the hysteresis losses and excess losses for alternating will increase further. This effect is not considered in the models by Zhu *et al.* (2019) and Abdi *et al.*(2021). To consider these effects in the loss modeling, different approaches have been developed. In a study by Belahcen *et al.* (2014), the hysteresis losses are segregated into two components, the alternating and the rotational hysteresis losses. In a study by Hernandez-Aramburo *et al.* (2003), a loss factor that depends on the axis ratio and peak flux density is multiplied by the sum of the calculated losses in two orthogonal unidirectional alternating fields. This loss factor is applied to the total iron losses and does not distinguish between the individual loss components. In a study by Ragusa *et al.* (2007), additional rotational loss factors r_{hyst} and r_{excess} are introduced to consider the effect on the iron losses under rotational magnetization, which provides the possibility to distinguish the effect of rotational magnetizations between the individual loss components. In a study by Steentjes *et al.* (2012), the IEM-5 parameter model was extended by these loss factors. In the simulation conducted by Steentjes *et al.* (2012), these factors were kept constant to $r_{\mathrm{hyst}} = r_{\mathrm{excess}} = 2.5$. Based on these empirical approaches by Ragusa *et al.* (2007) and Steentjes *et al.* (2012), a loss formulation based on unidirectional measurements at different angles to the rolling direction was introduced by Schauerte *et al.* (2019). In the context of the paper presented here, this loss formulation was further developed. The detailed theory of the adapted IEM loss model for rotational magnetization and detailed measurement results are presented in a study by Schauerte *et al.* (2021) as a preceding publication. In this paper, the adapted IEM loss model for rotational

magnetization is used for the iron loss calculation in a finite element method (FEM) simulation of an exemplary induction machine (IM) as it is done in studies by Abdi *et al.* (2021), Belahcen *et al.* (2014) and Hernandez-Aramburo *et al.* (2003). In addition, two frequently used frequency-based and one time-based model are used for the iron loss calculation in the FEM. The results of the simulated iron losses using these different loss models are compared. The differences of the adapted IEM loss model for rotational magnetization to the already established iron loss models are analyzed as well as the differences between all considered iron loss models.

The paper is structured as follows. First, in section 2 four different iron loss models are presented and discussed. The first three models are the modified Bertotti model, discussed in studies by Bertotti (1998) and Steentjes *et al.* (2012), the dynamic core loss model presented by Lin *et al.* (2004) and the IEM-5 parameter model presented by Steentjes *et al.* (2013a). The last one is the adapted IEM loss model for rotational magnetization that was developed in the context of this paper. Second, in section 3 the parameters and the simulation settings for an exemplary induction machine are introduced. Furthermore, the material parameters of the simulated steel sheet are listed. Third, in section 4 the analysis of the iron losses using the different iron loss models is conducted. For this analysis, the iron loss density in different locations in the stator and rotor of the machine is simulated and compared. The flux density loci in these locations differ from alternating to rotating magnetization.

2. Iron loss models

For the calculation of the iron losses, four different methods and approaches are considered in this paper. Three of them calculate the iron loss density in the frequency domain and one of them in the time domain.

For the use of the frequency-domain iron loss models in the postprocessing of the FEM simulation, the time-dependent flux density value $B(t)$ in each geometrical location in the machine is decomposed into its harmonics as discussed by Von Pfingsten *et al.* (2016). This results in a flux density value B_n for the fundamental component $n = 1$ and each harmonic component $n > 1$. The Fourier coefficients B_n are separated into the values in the rolling direction $B_{n,\mathrm{RD}}$ and the transverse direction $B_{n,\mathrm{TD}}$ of the iron sheet. Thus, a loss formulation such as:

$$P_{\mathrm{Fe}} = a\ B_{\mathrm{m}}^{\alpha}\ f + b\ B_{\mathrm{m}}^{2}\ f^{2} + c\ B_{\mathrm{m}}^{1.5}\ f^{1.5} \tag{1}$$

is transformed to:

$$\begin{aligned} P_{\mathrm{Fe}} = a \cdot & \left(\sum\nolimits_{n=1}^{\infty} \left(B_{n,\mathrm{RD}}^{2} + B_{n,\mathrm{TD}}^{2} \right)^{\frac{\alpha}{2}} \cdot nf \right) \\ + b \ \cdot & \left(\sum\nolimits_{n=1}^{\infty} \left(B_{n,\mathrm{RD}}^{2} + B_{n,\mathrm{TD}}^{2} \right) \cdot (nf)^{2} \right) \\ + c \ \cdot & \left(\sum\nolimits_{n=1}^{\infty} \left(B_{n,\mathrm{RD}}^{2} + B_{n,\mathrm{TD}}^{2} \right)^{\frac{1.5}{2}} \cdot (nf)^{1.5} \right), \end{aligned} \tag{2}$$

where a, b, c and α are loss parameters that are replaced by different loss parameters in the following section, B_{m} is the maximum flux density and f is the frequency. This means that rotating flux densities that occur are included and considered in the calculation. However, the effects described by Ragusa *et al.* (2007) and Appino *et al.* (2009) for rotating

magnetizations are not correctly covered. In the following, the loss models are presented in the form of equation (1). The separation into the rolling and transverse direction is also done in the time-domain iron loss model as explained in the next section.

2.1 Modified Bertotti loss model

The first iron loss model considered in this paper is the modified Bertotti model (Bertotti, 1998; Steentjes *et al.*, 2012):

$$P_{\mathrm{Fe,Bertotti}} = k_{\mathrm{hyst}}\ B_{\mathrm{m}}^{\alpha}\ f + k_{\mathrm{cl}}\ B_{\mathrm{m}}^{2}\ f^{2} + k_{\mathrm{exc}}\ B_{\mathrm{m}}^{1.5}\ f^{1.5} \tag{3}$$

which describes the iron loss densities in the frequency domain. In this model, k_{hyst}, k_{cl} and k_{exc} are the hysteresis, eddy current and excess loss factors fitted to the measurements (Steentjes *et al.*, 2012), B_{m} is the maximum magnetic flux density, f is the frequency and α is an additional loss parameter that is also approximated to the measurements. The strength of this model is its comprehensive physical explanation. A disadvantage of the modified Bertotti model is that it underestimates the losses at high magnetic flux densities and high frequencies, which is crucial in modern machine designs (Steentjes *et al.*, 2013a).

2.2 Dynamic core loss model

The second iron loss model is based on the Bertotti model and is introduced by Lin *et al.* (2004). The loss calculation is modeled in the time domain. The loss density results from the time average of the hysteresis $P_{\mathrm{hyst}}(t)$, eddy current $P_{\mathrm{cl}}(t)$ and excess loss $P_{\mathrm{exc}}(t)$ density and can be described by:

$$P_{\mathrm{Fe,Dyn}} = \frac{1}{T}\int_{t=t_0}^{t=t_0+T} \left(P_{\mathrm{hyst}}(t) + P_{\mathrm{cl}}(t) + P_{\mathrm{exc}}(t)\right)\ \mathrm{d}t \tag{4}$$

where t_0 is an arbitrary time and T the time period of the electromagnetic field.

In a certain geometry, the individual loss component is calculated by considering the flux density B_{RD} in the rolling direction and the flux density B_{TD} in transvers direction of the material:

$$P_{\mathrm{hyst}}(t) = \left(\left\|H_{\mathrm{irr}}\frac{\mathrm{d}B_{\mathrm{RD}}}{\mathrm{d}t}\right\| + \left\|H_{\mathrm{irr}}\frac{\mathrm{d}B_{\mathrm{TD}}}{\mathrm{d}t}\right\|\right) \tag{5}$$

$$P_{\mathrm{cl}}(t) = \frac{k_{\mathrm{cl}}}{2\pi^2}\cdot\left(\left\|\frac{\mathrm{d}B_{\mathrm{RD}}}{\mathrm{d}t}\right\|^2 + \left\|\frac{\mathrm{d}B_{\mathrm{TD}}}{\mathrm{d}t}\right\|^2\right) \tag{6}$$

$$P_{\mathrm{exc}}(t) = \frac{k_{\mathrm{exc}}}{C_{\mathrm{e}}}\cdot\left(\left\|\frac{\mathrm{d}B_{\mathrm{RD}}}{\mathrm{d}t}\right\|^2 + \left\|\frac{\mathrm{d}B_{\mathrm{TD}}}{\mathrm{d}t}\right\|^2\right)^{0.75} \tag{7}$$

where k_{hyst}, k_{cl} and k_{exc} are the hysteresis, eddy current and excess loss parameters of the modified Bertotti model and $C_{\mathrm{e}} = (2\pi)^{1.5}\cdot\frac{2}{\pi}\int_0^{\frac{\pi}{2}}\cos^{1.5}(\theta)\ \ \mathrm{d}\theta = 8.763363$. The irreversible component of the magnetic field strength H_{irr} is given by:

$$H_{\mathrm{irr}}(\theta) = \pm\frac{k_{\mathrm{hyst}}}{C_{\alpha}}\cdot\left\|B_{\mathrm{m}}\cos(\theta)\right\|^{\alpha-1} \tag{8}$$

with $C_\alpha = 4\int_0^{\pi/2} \cos^\alpha\theta \quad \mathrm{d}\theta$, $\theta = \arcsin\left(\frac{B}{B_\mathrm{m}}\right)$ and α being the additional loss parameter of the modified Bertotti model.

2.3 IEM-5-parameter loss model

The third loss model is also based on the modified Bertotti model and added by an additional term considering the nonlinear material behavior (Steentjes *et al.*, 2013a). With this IEM-5-parameter loss model, the loss determination at high magnetic flux densities and frequencies is improved compared to the modified Bertotti model. The IEM-formula is given by:

$$P_{\mathrm{Fe,IEM}} = a_1\ B_\mathrm{m}^{\alpha+\beta B_\mathrm{m}}\ f + a_2\ B_\mathrm{m}^2\ f^2 + a_5\ B_\mathrm{m}^{1.5}\ f^{1.5} + a_2\ a_3\ B_\mathrm{m}^{a_4+2}\ f^2 \tag{9}$$

where a_1, a_2 and a_5 are the hysteresis, eddy current and excess loss factors and a_2 and a_4 are loss parameters describing the nonlinear saturation losses. The model is validated in a study by Steentjes *et al.* (2013b). The IEM-formula, as well as the Bertotti model, have still the disadvantage that they do not consider rotational magnetization correctly and were developed for unidirectional magnetization. In the postprocessing of the FEM simulation, the nonlinear saturation losses are calculated by:

$$P_\mathrm{NL} = a_2\ a_3\ B_\mathrm{m}^{a_4+2} f^2 \tag{10}$$

where B_m is the maximum value of the flux density during one period. The hysteresis, eddy current and excess losses are calculated according to the principle in equation (2).

2.4 Adapted IEM loss model for rotational magnetization

To overcome the disadvantage that rotational magnetization is not adequately considered in the modified Bertotti model and IEM-formula, the fourth iron loss model is developed in the context of this paper, introduced in the study by Schauerte *et al.* (2021) as a preceding publication and given by:

$$\begin{aligned} P_{\mathrm{Fe,IEM,rot}} = {} & \left(1 - r_\mathrm{hyst}\ f_\mathrm{Ax}^2\right)\left(a_1 + a_{1,90^\circ}\ f_\mathrm{Ax}^{\alpha+\beta B_\mathrm{m}}\right) B_\mathrm{m}^{\alpha+\beta B_\mathrm{m}} f + a_2\left(1 + f_\mathrm{Ax}^2\right) B_\mathrm{m}^2\ f^2 \\ & + \left(1 - r_\mathrm{exc}\ f_\mathrm{Ax}^2\right)\left(a_5 + a_{5,90^\circ}\ f_\mathrm{Ax}^{1.5}\right)\ B_\mathrm{m}^{1.5}\ f^{1.5} + a_2 a_3\left(1 + f_\mathrm{Ax}^{a_4+2}\right) B_\mathrm{m}^{a_4+2}\ f^2 \end{aligned} \tag{11}$$

where a_1 and a_5 are the hysteresis and excess loss parameters in rolling and $a_{1,90^\circ}$ and $a_{5,90^\circ}$ those in transverse direction. The variable f_AX describes the axis ratio of the rotational magnetization.

The behavior of the hysteresis and excess loss components with respect to the peak polarization and the locus of the magnetic flux density is considered by the quadratic axis ratio f_Ax^2 and the additional factor r_hyst and r_exc, respectively. Both, hysteresis and excess losses, are based on domain wall movements. Nevertheless, as shown by Appino *et al.* (2016), the dependencies with respect to the peak polarization and the axis ratio differ for the two loss components. The analysis of this difference is only possible by quasi-static measurements. In this work, however, no measurement system is available which allows the detection of the rotating iron loss at quasi-static magnetization frequencies. Because the

parameterization of the iron loss model, which is described in more detail in the previous work (Schauerte *et al.*, 2021), was to be performed on the measurement system of the research group, an identical course was assumed due to the same phenomenological cause, the domain wall movement. More details on the adapted IEM loss model for rotating magnetization is given in the previous paper. The 2 D loss parameters r_{hyst} and r_{exc} are calculated by:

$$r_{\mathrm{hyst,exc}} = B_{\mathrm{m}} \cdot \frac{P_{\mathrm{Fe}}(J_{\mathrm{m}})}{B_{\mathrm{s}} \cdot P_{\mathrm{Fe}}(J_s)} \tag{12}$$

and shown in Figure 1. In equation (12), J_{m} is the polarization, J_{s} the saturation polarization, $P_{\mathrm{Fe}}(J_{\mathrm{m}})$ the identified iron loss density by averaged unidirectional measurements in all directions and $P_{\mathrm{Fe}}(J_{\mathrm{s}})$ the approximated saturated iron losses for $J_{\mathrm{m}} = J_{\mathrm{s}}$.

2.4.1 Measurement results of the adapted IEM loss model for rotational magnetization. To validate the adapted IEM loss model for rotational magnetization, the iron losses calculated with equation (11) are compared with measurement results. The measurements are performed with a rotational single sheet tester (RSST). More detailed explanations of the measurement setup and measurement procedure are described in the previous paper (Schauerte *et al.*, 2021). The waveform of each magnetic flux density location is determined by the maximum excitation B_{m}, the axial ratio f_{Ax} and the angle θ between the major axis of the ellipsoid and the rolling direction. The loss parameters in equation (11) necessary for modeling the iron losses and their individual components are determined by unidirectional measurements in rolling and transverse directions and are listed in Table 2. The comparison between measurement and simulation with additional decomposition of the individual loss components is shown in Figure 2. The measurements were performed for a frequency of $f =$ 400 Hz at different flux densities and axis ratios. The comparison of the measurement and simulation results shows a good agreement across the entire range of measurement parameters. It can be seen that the hysteresis and excess losses increase for an axis ratio of $f_{\mathrm{AX}} = 0.5$ compared to $f_{\mathrm{AX}} = 0.0$ across the entire range of flux densities. For rotating magnetization, the hysteresis and excess losses decrease as expected for high-flux densities. It must be emphasized here that the simulated behavior above 1.5 T is an extrapolation of the expected material behavior. The simulated losses in this range are an extrapolation of the measured data based on the behavior described in the literature. Further analysis of the measurement and simulation results of the adapted IEM loss model for rotating magnetizations are given by Schauerte *et al.* (2021).

3. Simulation of an exemplary machine

The proposed iron loss models are used in a FEM simulation of an exemplary aluminum die-cast squirrel cage IM. The cross-sectional area and important geometrical and electrical parameters are given in Figure 3.

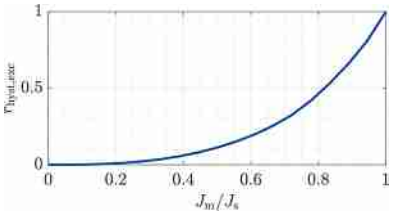

Figure 1.
2 D-loss parameters r_{hyst} and r_{exc}

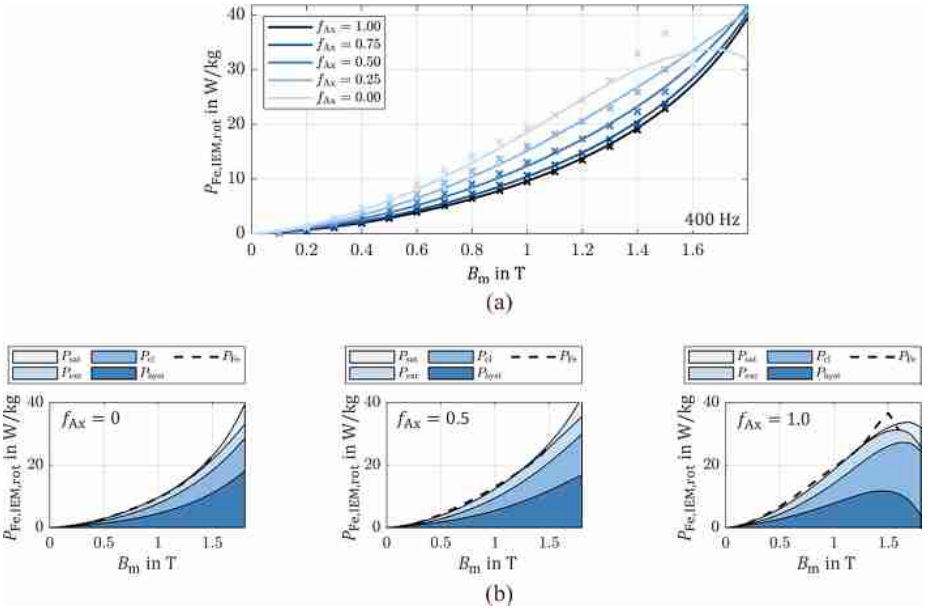

Figure 2.
Measured (crosses) and simulated (solid lines) iron loss for increasing axis ratios f_{Ax} (a) simulated iron loss components vs measurements (dashed line) and (b) at 400 Hz for $\theta = 0°$ (Schauerte *et al.*, 2021)

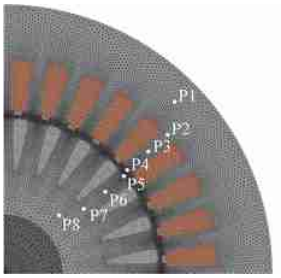

Parameter		Value	Unit
number of pole pairs	p	2	-
number of stator slots	N_S	36	-
number of rotor slots	N_R	28	-
outer stator diameter	$d_{S,O}$	170	mm
outer rotor diameter	$d_{R,O}$	102	mm
air gap width	δ	0.5	mm
active iron length	l_{Fe}	200	mm
number of pole pairs	p	2	-
DC link voltage	U_{DC}	130	V
maximum phase current	$I_{Phase,max}$	350	A

Figure 3.
Cross-sectional area, machine parameters and geometrical locations in the IM

The iron loss density is simulated in four different locations (P1 to P4) of the stator lamination and four different locations (P5 to P8) in the rotor lamination. The different geometrical locations in the machine are defined in Figure 3. They can be grouped regarding to the appearance of the magnetic flux density. At the points P1 and P8, that are in the yoke of the stator and rotor, and the points P3 and P6, that are in the middle of the stator and rotor tooth, respectively, unidirectional magnetization occurs. The magnetic flux density in the points of the yoke is smaller compared to those in the teeth. The locations P2 and P7 are located at the transition from the tooth to the yoke where typically rotational magnetization occurs. The locations P4 and P5 are at the stator and rotor tooth tip, where high harmonics of the flux density occur.

Furthermore, the analysis is performed for four different operating points of the IM. The operating points are shown in Figure 4. Operating Point OP4 and OP3 are in the field weakening range, resulting in a reduced flux density compared to the operating points OP2

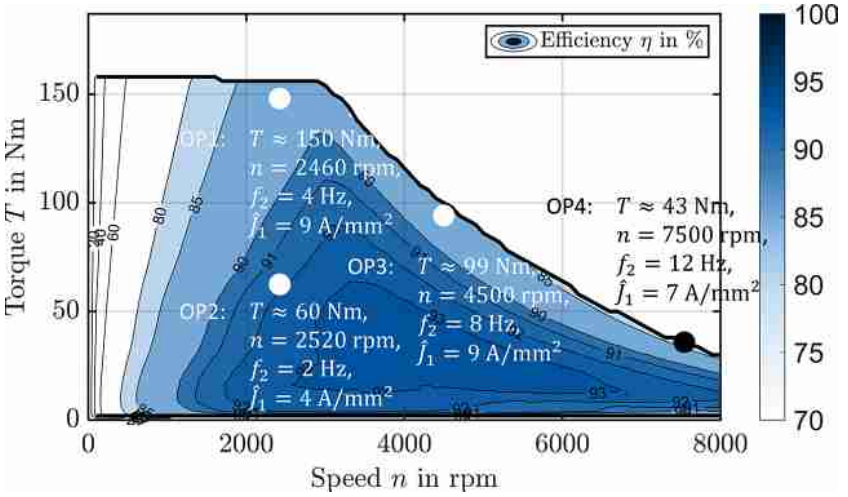

Figure 4.
Operating points of the IM used for the iron loss analysis

and OP1 in the base speed range. Due to the higher amount of current, the flux density in OP1 is higher compared to those in OP2.

Both the stator and the rotor of the IM are constructed of thin, stacked and electrically insulated electrical sheets. For this reason, the magnetic flux density in the axial direction of the machine is neglected in the simulations. Thus, for the analysis considered here, a 2 D simulation of the machine is sufficient. The simulation of the IM is performed using a current-driven 2 D FEM. The solver used is IEM's in-house solver iMOOSE/pyMOOSE considering a magnetoquasistatic formulation over the magnetic vector potential. The magnetic material characteristic of the stator and rotor laminations is considered by a reluctivity $\nu(B)$ based on material measurements. The nonlinear field problem is solved by a Newton–Raphson procedure. The mesh consists of 28,000 elements of first order with a variable mesh size as it can be seen in Figure 3. The air gap is divided into three layers.

The stator frequency in the simulation is set to the corner point stator frequency of $f_1 =$ 86 Hz. The stator slot current density J_1 and the rotor current frequency f_2 differ from operating point to operating point. The sampling frequency is chosen to $f_{\text{samp}} = 10$ kHz to consider the losses due to high harmonics as discussed by Von Pfingsten *et al.* (2018). The values for the different operating points are listed in Table 1.

The material of the stator and rotor lamination was metrologically characterized beforehand by using a single sheet tester (SST) and an RSST, which was developed to characterize the iron losses under the influence of rotating magnetization (Müller *et al.*, 2019; Appino *et al.*, 2016 ; Thul *et al.*, 2018). The measurements are used to identify the loss

#	$\hat{J}_1$ in A/mm^2	f_1 in Hz	f_2 in Hz	f_{sw} in kHz
1	4	86	2	10
2	9	86	4	10
3	9	86	8	10
4	7	86	12	10

Table 1.
Simulation parameters for the different operating points

parameters of the four different proposed iron loss models. The identified loss parameters are listed in Table 2.

4. Iron loss simulation results

As examples for the behavior of the iron losses in different saturated operating points of the machine, the results of operating point OP4 in the field weakening range and OP1 in the base speed range are shown in the following. The flux density in OP4 is significantly lower than in OP1.

The flux density in the stator and rotor lamination as well as the flux density loci in the different geometrical locations in the machine for operating point OP4 are shown in Figure 5. The maximum achieved flux density in this field weakening operating point occurs in the stator and rotor tooth tips and is $B_{\mathrm{m}} \approx 1.5\,\mathrm{T}$. In the locations P1, P3 and P6, unidirectional magnetizations with a low axis ration $f_{\mathrm{AX}} < 0.1$ and flux density values below 1 T occur. The maximum flux density in the stator tooth location P3 is ca. 1 T, in the stator yoke location P3 is ca. 0.8 T and in the rotor tooth location is ca. 0.7 T. In points P2, P7 and P8, elliptical and rotational magnetization with high axis ratios $f_{\mathrm{AX}} > 0.55$ and flux density

Table 2.
Identified loss parameters for the used iron loss models

Loss Modell	a_1	a_2	a_3	a_4	a_5	$a_{1,90°}$	$a_{5,90°}$	α	β
Bertotti	0.011260	2.1650×10^{-5}	–	–	0.0002	–	–	2.2840	–
Dynamic	0.011260	2.1650×10^{-5}	–	–	0.0002	–	–	2.2840	–
IEM	0.010845	2.1355×10^{-5}	0.005837	7.8138	0.0002	–	–	1.5235	0.5649
IEM Rot	0.010845	2.1355×10^{-5}	0.005837	7.8138	0.0002	0.01202	0.0003	1.5235	0.5649

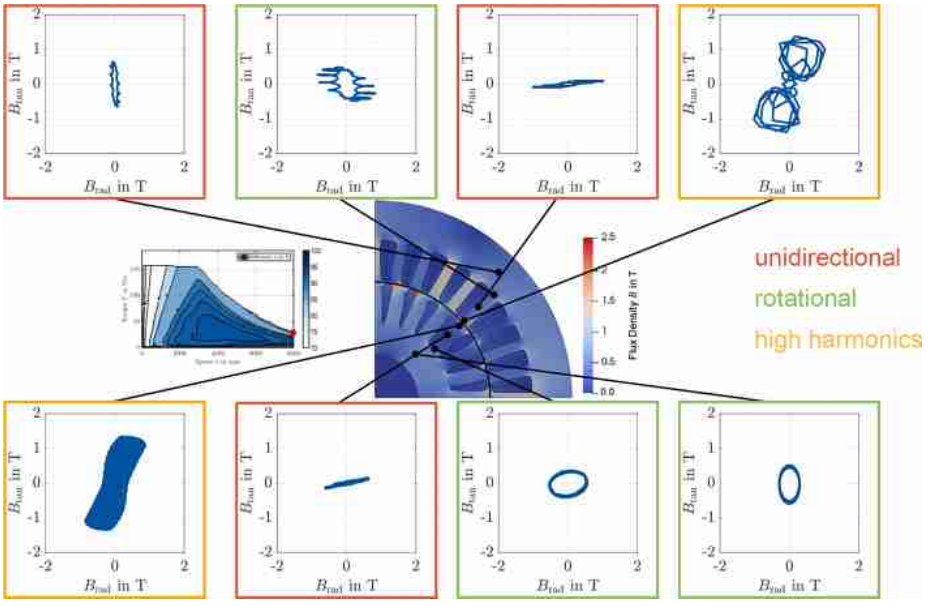

Figure 5.
Flux density loci in different geometrical locations in the machine for operating point OP4

values below 1 T occur. The maximum flux density at the transition of the stator tooth and stator yoke P2 is ca. 0.8 T, at the transition of the rotor tooth and rotor yoke P7 is ca. 0.6 T and in the rotor yoke location is ca. 0.6 T. In the geometrical locations P4 and P5, the flux density loci include a high number of harmonics. Additionally, the flux density values reach values higher than 1 T. Therefore, in this operating point OP4, the locations P1, P3 and P6 can be grouped to points with an unidirectional magnetization with low magnetic flux density values that are less than 1 T. The locations P2, P7 and P8 are grouped to points with an elliptical magnetization and low magnetic flux density values. The locations P4 and P5 are points of high oscillating flux density with values larger than 1 T.

For operating point OP3, the different locations can be grouped in the same mentioned groups than those of operating point OP4. The flux densities in each location for OP3 are slightly higher than in OP4, but still keep within the mentioned limits. Therefore, visualization of the B loci at this operating point is omitted.

The simulated iron loss densities for operating point OP4 are shown in Figure 6. It can be noted that the calculated iron loss densities in the group of the locations with unidirectional magnetization and low-flux density values using the IEM-Formula [IEM (9)] and the adapted IEM loss model for rotational magnetization [Adapted IEM (11)] are equal. This corresponds to the measurement results in study by Schauerte *et al.* (2021). For rotational magnetization with an axis ratio value $f_{Ax} \gg 0$, the use of the adapted IEM loss model for rotational magnetization results in higher iron loss density, particularly for the hysteresis and excess loss components, than the IEM-Formula. This shows that the increase of hysteresis and excess losses in case of rotational magnetization and flux density values less than 1 T is accurately considered in the simulation. In the most geometrical locations, the losses calculated using the Bertotti and the dynamic core loss model are less than the ones calculated with the IEM-Formula and the adapted IEM loss model for rotational magnetization. These models underestimate the losses at the high frequencies of the harmonics and higher flux densities. In the locations P7 and P8, where flux density values are less than 0.5 T and a low number of harmonics occur, the Bertotti [Bertotti (3)] and dynamic core loss model [Dynamic (4)] yield quite the same loss densities than the IEM-

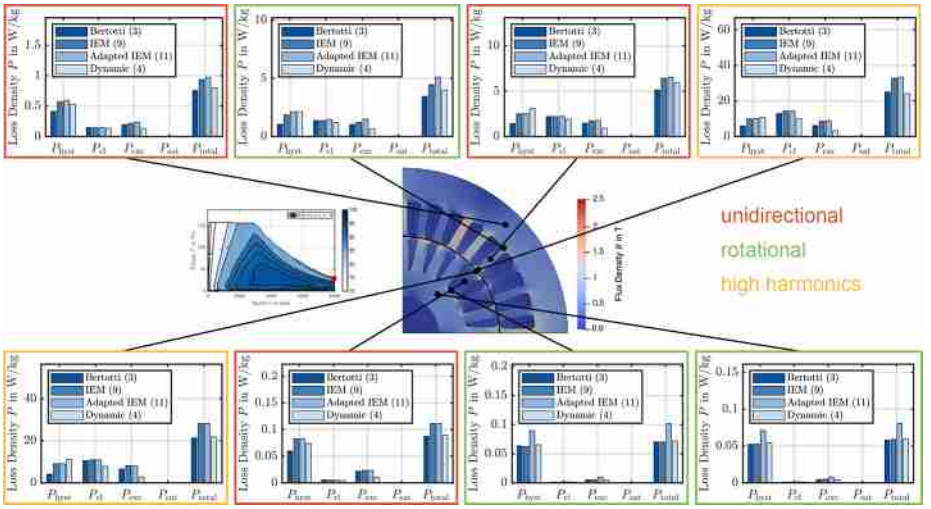

Figure 6.
Simulated iron loss densities for operating point OP4

Formula, which was expected (Eggers *et al.*, 2017). In case of a high number of harmonics, the dynamic core loss model results in higher hysteresis loss densities than the Bertotti model, as it can be seen in P4 and P5. The assumption of a sinusoidal excitation for the transformation of the hysteresis losses in the Bertotti model in the frequency domain to those in the dynamic core loss model in the time domain is violated. This can also be observed in further locations with harmonics in the flux density such as locations P1, P2 or P3.

As the flux density profiles in operating point OP3 can be divided into the same groups as those of operating point OP4, the simulated iron loss densities at the various locations in OP3 behave quite similarly to the loss densities in OP4. Therefore, the visualization of the simulated iron loss densities for operating point OP3 is omitted here as well.

In Figure 7, the flux density in the stator and rotor lamination as well as the flux density loci in the different geometrical locations in the machine for operating point OP1 are shown. The maximum achieved flux density in this base speed operating point also occurs in the stator and rotor tooth tips and is $B_{\mathrm{m}} > 1.5\,\mathrm{T}$. In the locations P3 and P6, unidirectional magnetizations with a low axis ration $f_{\mathrm{AX}} < 0.06$ and flux density values over 1.5 T occur. The maximum flux density in the stator tooth location P3 is ca. 1.95 T and in the rotor tooth location is ca. 1.9 T. The flux density in location P1 is not unidirectional as in operating point OP4 and has an axis ratio of $f_{\mathrm{Ax}} \approx 0.23$. The maximum achieved flux density in this location is ca. 1.9 T. In points P2, P7 and P8, rotational magnetization with axis ratios $f_{\mathrm{AX}} > 0.75$ and flux density values over 1.5 T occur. The maximum flux density at the transition of the stator tooth and stator yoke P2 is ca. 1.85 T, at the transition of the rotor tooth and rotor yoke P7 is ca. 1.8 T and in the rotor yoke location is ca. 1.75 T. As in operating point OP4, the flux density loci in the geometrical locations P4 and P5 include a high number of harmonics and the flux density reaches values higher than 1.5 T. In this operating point, the locations P3 and P6 can be grouped to points with an unidirectional magnetization with high

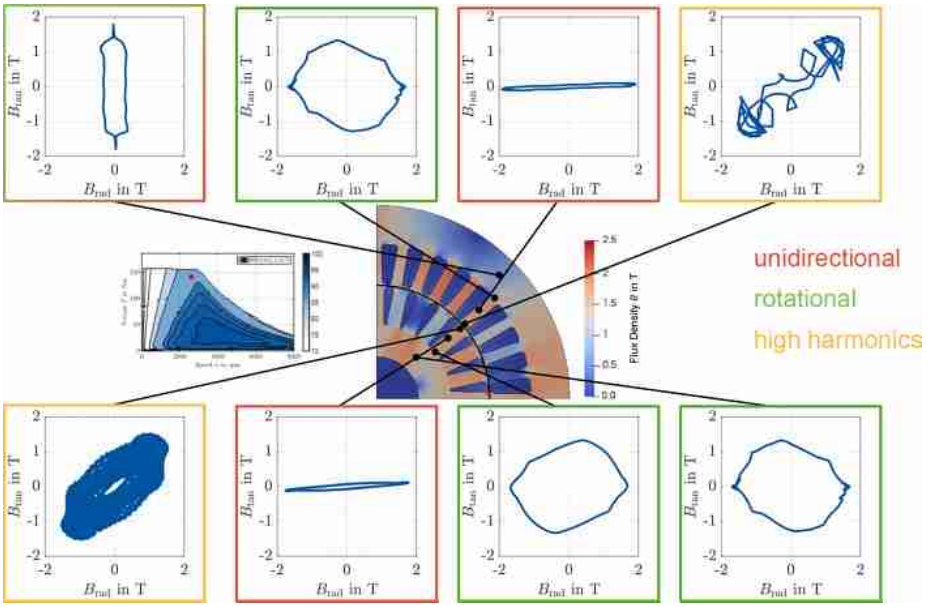

Figure 7.
Flux density loci in different geometrical locations in the machine for operating point OP1

magnetic flux density values that are more than 1.5 T. The locations P2, P7 and P8 are grouped to points with a rotational magnetization and high magnetic flux density values that are more than 1.5. The location P3 is in between of these groups. As in operating point OP3, the locations P4 and P5 are points of high oscillating flux density values larger than 1 T.

For operating point OP2, the different locations can be grouped in the same mentioned groups than those of operating point OP1. The flux densities in each location for OP2 are slightly lower than in OP4, but still keep within the mentioned limits. Therefore, visualization of the B loci at this operating point is also omitted.

The simulated iron loss densities for operating point OP1 are shown in Figure 8. On the one hand, it can be noted that the calculated iron loss densities in the group of the locations with unidirectional magnetization and high-flux densities using the IEM-Formula [IEM (9)] and the adapted IEM loss model for rotational magnetization [Adapted IEM (11)] are equal, as it is in the operating point OP4. This also corresponds to the measurement results by Schauerte *et al.* (2021). On the other hand, for the rotational magnetization with axis ratio values $f_{AX} > 0.75$, the results of the adapted IEM loss model for rotational magnetization in OP1 show lower iron loss densities, particularly for the hysteresis and excess loss components, than the results of the IEM-Formula and the other iron loss models. This is the opposite behavior than in OP4. The effect that, in the case of rotational magnetization, the hysteresis and excess losses are decreasing for high magnetic flux densities are well considered in this simulation.

In all geometrical locations, the losses calculated using the Bertotti [Bertotti (3)] and the dynamic core loss model [Dynamic (4)] are less than the ones calculated with the IEM-Formula and the adapted IEM loss model for rotational magnetization. These models underestimate the losses at the high frequencies of the harmonics and higher flux densities. The disadvantage of the Bertotti and dynamic core loss model, that the losses at high-flux densities are underestimated, is clearly shown here. In case of a high number of harmonics, as it occur in location P4 and P5, the dynamic core loss model also results in significant higher hysteresis losses compared to the Bertotti model.

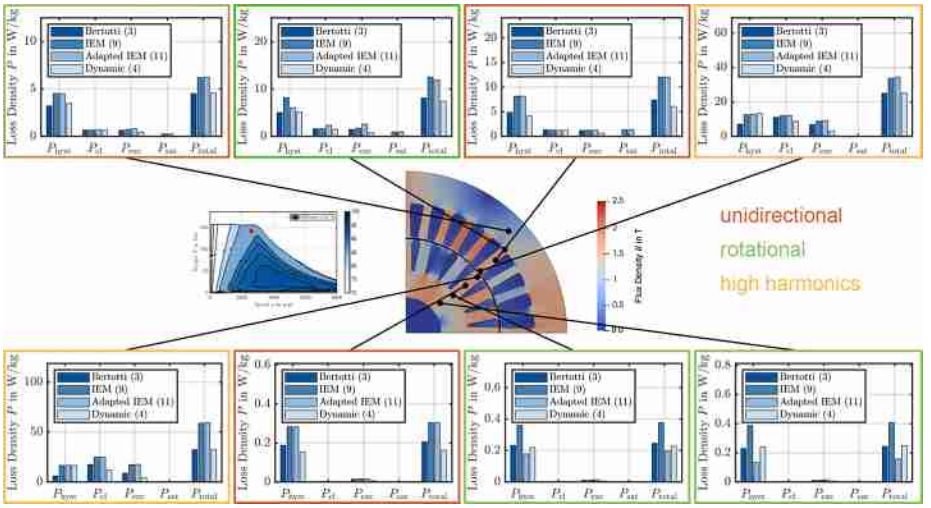

Figure 8.
Simulated iron loss densities for operating point OP1

As the flux density profiles in operating point OP3 can be divided into the same groups as those of operating point OP4, the simulated iron loss densities at the various locations in OP3 behave similarly to the loss densities in OP4. Therefore, the visualization of the simulated iron loss densities for operating point OP3 is omitted here as well.

5. Conclusions

In this paper, a frequency-based iron loss model to consider the effect on the iron losses under rotational magnetization is used in a FEM simulation of an exemplary IM. This adapted IEM loss model for rotational magnetization is developed in the context of this paper and presented in detail in study by Schauerte *et al.* (2021) as a preceding publication. The simulated iron losses are analyzed and compared with the results of FEM simulations using other already established loss models. These further loss models are the frequency-based modified Bertotti model and the IEM-5 parameter model and the time-based dynamic core loss model.

For the analysis, the iron loss density at different locations within the rotor and stator laminations are used for different operating points. The locations differ in the magnetization that occurs. Locations with alternating and rotating flux densities are considered as well as locations with a high amount of harmonics.

The modified Bertotti model, the IEM-5 parameter model and the dynamic core loss model underestimate the hysteresis and excess losses in locations of rotational magnetizations and low-flux densities, while they overestimate the losses for rotational magnetization and high-flux densities. In contrast, the effects of rotating magnetization are considered in the adapted IEM loss model for rotational magnetization. For unidirectional magnetization as well as for magnetizations with a high amount of harmonics, the adapted IEM loss model for rotational magnetization gives quite similar results to the IEM-5 parameter model. Furthermore, it is shown that the dynamic core loss model presented in this paper results, compared to the Bertotti model and IEM-5 parameter model, in significant higher hysteresis losses for magnetizations with a high amount of harmonics.

The results thus show that the developed adapted IEM loss model for rotational magnetization can be used to simulate electrical machines and reproduce the effects of rotational flux densities within a machine simulation.

References

Abdi, S., Abdi, E. and Mcmahon, R. (2021), "A new iron loss model for brushless Doubly-Fed machines with hysteresis and field rotational losses", *IEEE Transactions on Energy Conversion*, Vol. 36 No. 4, pp. 3221-3230, doi: 10.1109/TEC.2021.3075629.

Appino, C., Fiorillo, F. and Ragusa, C. (2009), "One-dimensional/two-dimensional loss measurements up to high inductions", *Journal of Applied Physics*, Vol. 105 No. 7, p. 07E718, doi: 10.1063/1.3068540.

Appino, C., Khan, M., De La Barriere, O., Ragusa, C. and Fiorillo, F. (2016), "Alternating and rotational losses up to magnetic saturation in non-oriented steel sheets", *IEEE Transactions on Magnetics*, Vol. 52 No. 5, pp. 1-4, doi: 10.1109/TMAG.2016.2528338.

Belahcen, A., Rasilo, P. and Arkkio, A. (2014), "Segregation of iron losses from rotational field measurements and application to electrical machine", *IEEE Transactions on Magnetics*, Vol. 50 No. 2, pp. 893-896, doi: 10.1109/TMAG.2013.2284606.

Bertotti, G. (1998), *Hysteresis in Magnetism: For Physicists, Materials Scientists, and Engineers*, Academic Press.

Eggers, D., Steentjes, S. and Hameyer, K. (2017), "Advanced iron-loss estimation for nonlinear material behavior", *IEEE Transactions on Magnetics*, Vol. 48 No. 11, pp. 3021-3024, doi: 10.1109/TMAG.2012.2208944.

Hernandez-Aramburo, C.A., Green, T.C. and Smith, A.C. (2003), "Estimating rotational iron losses in an induction machine", *IEEE Transactions on Magnetics*, Vol. 39 No. 6, pp. 3527-3533, doi: 10.1109/TMAG.2003.819451.

Kowal, D., Sergeant, P., Dupré, L. and Vandenbossche, L. (2015), "Comparison of iron loss models for electrical machines with different frequency domain and time domain methods for excess loss prediction", *IEEE Transactions on Magnetics*, Vol. 51 No. 1, pp. 1-10, doi: 10.1109/TMAG.2014.2338836.

Krings, A. and Soulard, J. (2010), "Overview and comparison of iron loss models for electrical machines", *5th International Conference and Exhibition on Ecological Vehicles and Renewable Energies (EVER 10)*, *Monte-Carlo, Monaco*, MAR 25-28.

Lin, D., Zhou, P., Fu, W.N., Badics, Z. and Cendes, Z.J. (2004), "A dynamic core loss model for soft ferromagnetic and power ferrite materials in transient finite element analysis", *IEEE Transactions on Magnetics*, Vol. 40 No. 2, pp. 1318-1321, doi: 10.1109/TMAG.2004.825025.

Müller, F., Bavendiek, G., Schauerte, B. and Hameyer, K. (2019), "Measurement and simulation of a rotational single sheet tester", *Archives of Electrical Engineering*, Vol. 68 No. 1, pp. 173-183, doi: 10.24425/aee.2019.125988.

Nell, M., Schauerte, B., Brimmers, T. and Hameyer, K. (2021), "Analysis of simulated iron losses in electrical machines by using different iron loss models", paper presented at the XXVI Symposium of Electromangetic Phenomena in Nonlinear Circuits (EPNC), April 7-9, Torino, Italy, Online Conference.

Ragusa, C., Appino, C. and Fiorillo, F. (2007), "Magnetic losses under two-dimensional flux loci in Fe–Si laminations", *Journal of Magnetism and Magnetic Materials*, Vol. 316 No. 2, pp. 454-457, doi: 10.1016/j.jmmm.2007.03.170.

Schauerte, B., Steentjes, S., Thul, A. and Hameyer, K. (2019), "Iron-loss model for arbitrary magnetization loci in NO electrical steel", *International Journal of Applied Electromagnetics and Mechanics*, Vol. 61 NO. S1, pp. S89-S96, doi: 10.3233/JAE-191599.

Schauerte, B., Nell, M., Leuning, N. and Hameyer, K. (2021), "Adaption and parametrization of an iron-loss model for rotating magnetization loci in NO electrical steel", paper presented at the XXVI Symposium of Electromangetic Phenomena in Nonlinear Circuits (EPNC), April 7.-9, Torino, Italy, Online Conference.

Steentjes, S., Leßmann, M. and Hameyer, K. (2012), "Advanced Iron-Loss calculation as a basis for efficiency improvement of electrical machines in automotive application", *Electrical Systems for Aircraft, Railway and Ship Propulsion (ESARS 2012)*, *Bologna, Italy*, pp. 1-6, doi: 10.1109/ESARS.2012.6387502.

Steentjes, S., Lemann, M. and Hameyer, K. (2013a), "Semi-physical parameter identification for an iron-loss formula allowing loss-separation", *Journal of Applied Physics*, Vol. 113 No. 17, pp. 17A319-17A319-3, doi: 10.1063/1.4795618.

Steentjes, S., von Pfingsten, G., Hombitzer, M. and Hameyer, K. (2013b), "Iron-loss model with consideration of minor loops applied to FE-Simulations of electrical machines", *IEEE Transactions on Magnetics*, Vol. 49 No. 7, pp. 3945-3948, doi: 10.1109/TMAG.2013.2244072.

Thul, A., Steentjes, S., Schauerte, B., Klimczyk, P., Denke, P. and Hameyer, K. (2018), "Rotating magnetizations in electrical machines: measurements and modeling", *AIP Advances*, Vol. 8 No. 5, p. 056815, doi: 10.1063/1.5007751.

Von Pfingsten, G., Nell, M. and Hameyer, K. (2018), "Hybrid simulation approaches for induction machine calculation", *COMPEL – The International Journal for Computation and Mathematics*

in Electrical and Electronic Engineering, Vol. 37 No. 5, pp. 1744-1754, doi: 10.1108/COMPEL-01-2018-0015.

Von Pfingsten, G., Ruf, A., Steentjes, S. and Hameyer, K. (2016), "Operation mode dependent requirements on magnetic properties of NO electrical steel in traction drives", *ser. Tagungsband – Aachener Stahlkolloquium – Umformtechnik., Verlagshaus Mainz GmbH Aachen, Gerhard Hirt (Hrsg.), no. 1*, pp. 163-176.

Zhu, Z.-Q., Xue, S., Chu, W., Feng, J., Guo, S., Chen, Z. and Peng, J. (2019), "Evaluation of iron loss models in electrical machines", *IEEE Transactions on Industry Applications*, Vol. 55 No. 2, pp. 1461-1472, doi: 10.1109/TIA.2018.2880674.

Corresponding author
Martin Marco Nell can be contacted at: martin.nell@iem.rwth-aachen.de